

Spectropolarimetry of Broad H α Lines and Geometry of the BLR

Marshall H. Cohen

California Institute of Technology, Pasadena, CA 91125

André R. Martel

Johns Hopkins University, 3400 N. Charles Street, Baltimore, MD 21218

Abstract. In a small fraction of Broad Line Radio Galaxies (BLRG) and Seyfert 1 galaxies, the polarization position angle rotates across the broad emission lines, especially at H α . An understanding of this behavior can potentially yield important information on the scattering geometry in the nucleus. We show two examples of this phenomenon, 3C 445, a BLRG, and Mrk 231, a Seyfert 1, and present an equatorial scattering model that explains some of its features in a straightforward way.

1. Introduction

The literature contains a number of examples of rotation of the polarization position angle (PA) in H α in Seyfert 1 galaxies and in broad-line radio galaxies (BLRG). This has usually been explained as radiation from the nuclear sources (continuum and BLR) being scattered from separated clouds, so that different Doppler-shifted wavelengths are seen at different PA . The most elaborate discussion of this is by Martel (1998) who decomposed H α in NGC 4151 into components each with its own PA . Several of the components were able to be associated with various features in the galaxy. Such an interpretation, dominated by radial motions, suffers from a lack of knowledge of the relative location and velocities of the emitters and scatterers.

In this paper we investigate a different possibility, that the rotations are caused by scattering of H α radiation on nearby clouds which see both red- and blue- shifted radiation but from different directions. The scattering planes are different for the red- and blue- shifted rays and an integration gives a PA that can rotate through H α . A discussion of this idea is in Cohen et al. (1999; hereafter C99) and it is mentioned by Goodrich and Miller (1994).

2. Examples

2.1. Mrk 231

Figure 1 shows (a) total flux, (b) polarization P , and (c) position angle PA for the H α region of Mrk 231 (Martel 1996; hereafter M96) and 3C 445 (C99). Note that P is S-shaped in Mrk 231, decreasing on the blue side and increasing on

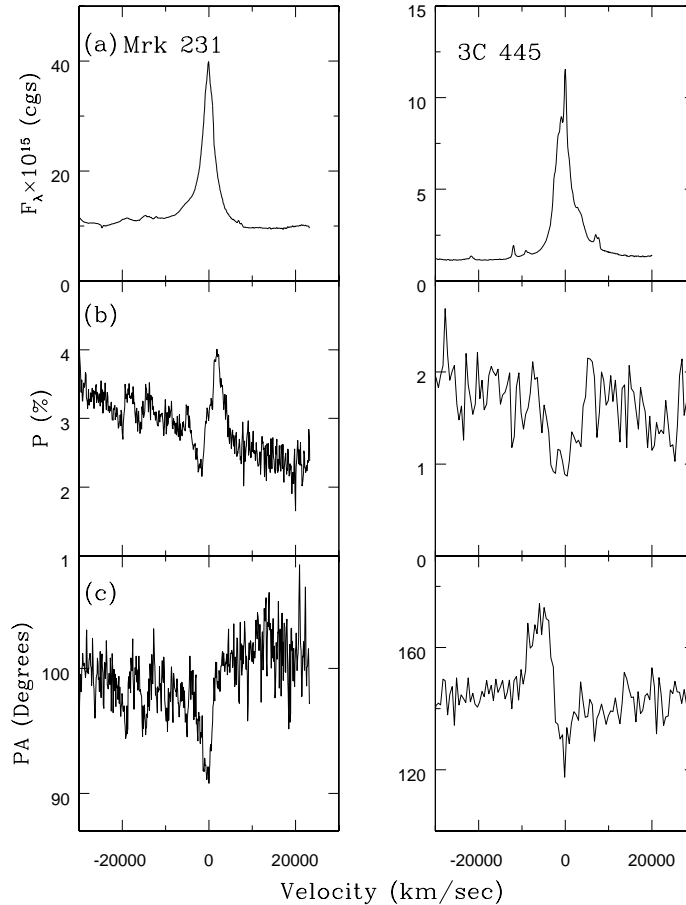


Figure 1. $H\alpha$ spectral region of Mrk 231 and 3C 445 : (a) total flux (b) percentage polarization (c) PA . Note the S-shaped changes in P in Mrk 231 and in PA in 3C 445.

the red side of $H\alpha$. This shows that the PA of the $H\alpha$ flux is different in the two wings; and that either P is higher in $H\alpha$ than in the continuum, or (more likely) that the dilution of P by unpolarized components is lower in (continuum + $H\alpha$) than in the continuum alone. In (c), it can be seen that the PA of $H\alpha$ is similar to that of the continuum in most of the red wing, but PA (blue) is smaller. In fact the intrinsic (continuum-corrected) shift in PA (blue) must be rather substantial, because in (b) the dip in the blue is nearly as big as the rise in the red. M96 modelled this line with 5 Gaussian components, each with its own wavelength and PA . His result is that there is a trend in PA corresponding to velocity, and the PA difference between the red and blue wings is about 30° .

2.2. 3C 445

Spectra for the BLRG 3C 445 are shown in the right-hand panels of Figure 1 (C99). The polarization fraction P has a weak S pattern, but PA has striking changes across $H\alpha$. A decomposition of the flux into line and continuum com-

ponents (C99) shows that $PA(H\alpha)$ has about a 45° change from the red to the blue wing, and much of the change occurs about 2500 km s^{-1} to the blue of the line center.

2.3. Others

The $H\alpha$ polarization in seven Sey 1 galaxies is discussed in M96. For most, the continuum and line polarizations are low, $\sim 1\%$, and they all show structure across their $H\alpha$ profiles in both P and PA . Mrk 304 and NGC 3516 are similar to Mrk 231 in having a strong S shape in P , and the S pattern is offset to the blue by perhaps 2500 km s^{-1} in Mrk 304. As for Mrk 231, the PA also changes where P dips. In Mrk 704, the PA rotates about 8° across the central 5500 km s^{-1} of $H\alpha$. A few BLRG, in addition to 3C 445, show polarization changes in $H\alpha$. 3C 227 has both $H\alpha$ and $H\beta$ offset by $\sim 20^\circ$ from the continuum; in this case the PA of the line radiation itself is approximately constant (C99).

Many broad-absorption-line quasars show PA rotations (Ogle 1998, Ogle et al. 1999), especially in the deep absorption troughs. It is not clear if these rotations are generically similar to those seen in the emission lines of BLRG and Seyfert 1's.

3. An Equatorial Model

Figure 2 shows the equatorial plane of an idealized AGN. $H\alpha$ -emitting clouds orbit with velocity v on the inner circle of radius r , and scattering clouds lie on the outer circle of radius R ($\rho = r/R$). Both the $H\alpha$ and scattering clouds are uniformly distributed around the circles, and the former radiate isotropically. The observer is in the $y - z$ plane at angle θ from the z -axis. AGN unification scenarios generally assume that BLRG are seen near the boundary of an obscuring dusty torus, which shields the central quasar from direct view. In Figure 2, the projection of the torus' edge on the equatorial plane is represented by arc AC and the dashed region is hidden, and the observer has an asymmetric view of the equatorial plane. The asymmetry is necessary to obtain rotation of the PA , and also for the model to mimic the observed spread between the optical continuum PA and the radio axis, which we assume to be projected onto the y axis. Point B receives both red- and blue-shifted radiation but the scattering planes are different so the red and blue wings of the scattered line will be at different position angles. When this is integrated over the visible arc ABC, the PA can rotate as a function of velocity.

Dust is much more efficient than electrons at scattering and so we take R to be at the inner wall of the dusty torus. If this is near 1 pc and the BLR is at a few light months, then $\rho \sim 0.1$. This picture is very simplified since in reality the torus will be irregular (think of the Galactic Center). It would be more realistic to put clouds randomly near the outer circle and to vary R ; and also of course to add structure in the z direction for both the emission and scattering clouds. These elaborations are not warranted at present.

In the examples shown below, we have taken $\rho = 0.1$ and the only free parameters are θ and the points A and C which define the visible arc. In fact, a wide range of results can be obtained by varying A and C, essentially because the integration adds together many vectors with a wide range of angles, and the

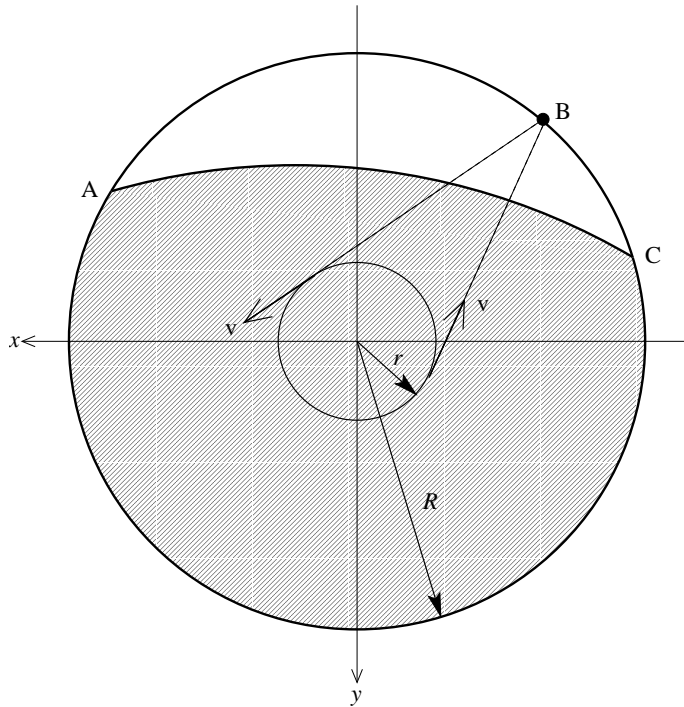


Figure 2. Equatorial plane of an AGN viewed along the z -axis. $H\alpha$ clouds orbit with velocity v on the inner circle. Emission from the clouds is scattered by material on the outer circle and is seen by an observer at angle θ from the z -axis. A dusty torus hides the hatched region from direct view. At point B, the scattering planes are different for the blue and red rays, and the observed blue and red polarizations are at different PA 's.

(often small) residual vector can depend critically on the details of cancellation. For the results shown here we weigh radiation in the equatorial plane by the inverse square of the distance and with a cosine that makes the opposite point invisible.

Light from the central continuum source, which has no motions in our model, will also be scattered from the arc ABC, and its PA will be the same as that of the zero-velocity point of $H\alpha$. However, in some AGN these PA 's differ. This can be accommodated in our model by adding another velocity, an outflow of $H\alpha$, or circular or radial motions of the scatterers. This opens up a wide range of parameter space which we have explored only in a limited fashion. Here, we only discuss models where the $H\alpha$ clouds have circular motions and the scatterers are stationary.

If the arc ABC is strictly symmetric around the x or y axis then the continuum polarization will be parallel or perpendicular to the radio axis, respectively.

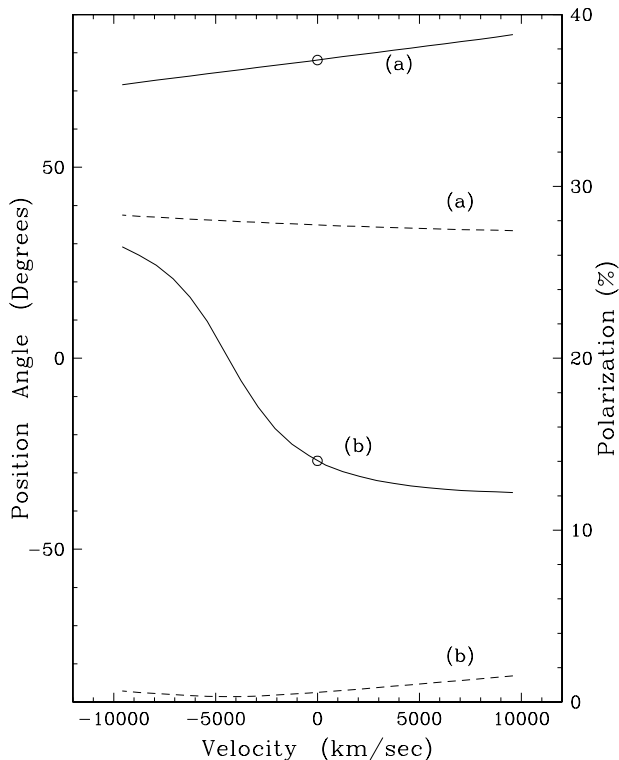


Figure 3. Calculations based on the model sketched in Figure 2 with $\rho = 0.1$, $\theta = 20^\circ$, and $v = 10,000 \text{ km s}^{-1}$. Solid curves are the position angle, and dotted curves are the percentage polarization, of the scattered $\text{H}\alpha$ radiation. (a) arc ABC is from 1.1π to 1.8π ; (b) arc ABC is from 1.05π to 2.0π . The open circles show the PA of the continuum.

But we expect that in general the x axis will be obscured and the arc will be more or less as shown. This means that radio-optical PA differences will avoid 0° , but values near 90° will not be common either. This is in accord with observations of BLRG; for five BLRG in C99 the median difference is 31° . If we take the radio axis to be given by the smallest-scale observations with the VLBA, and the optical PA to be that of the continuum near $\text{H}\alpha$, then the radio-optical differences for Mrk 231 and 3C 445 are 33° and 31° , respectively (M96; Ulvestad et al. 1999; C99)

4. Results

Figure 3 shows two examples of the many possibilities that can be obtained with the model. To compare them with observations (Fig. 1) it is necessary to combine $\text{H}\alpha$ and continuum components. In case (a), the PA rotates uniformly and the continuum PA is in the middle of the $\text{H}\alpha$ range. This results in an

S-shaped PA curve as in 3C 445. However, two features of the observation are inconsistent with the model: the measured curve is symmetric around -2500 km s^{-1} instead of 0 km s^{-1} , and the radio-optical PA difference is 31° , rather far from the model 75° . These discrepancies, especially the first, appear to be rather difficult to resolve; but adding a velocity, e.g. circular motion of the scatterers, introduces many possibilities including offsetting the PA of the zero-velocity component from the continuum. The polarization in the scattered light is high, nearly 30%, which is good because there also could be non-scattered components of both $H\alpha$ and continuum, which would dilute the polarization.

In case (b) the continuum PA is close to that of the red wing of $H\alpha$, and this gives P and PA curves like those in Mrk 231. The model radio-optical PA difference is 27° , close to the observed value of 33° . However, the cancellation of the vectors is nearly complete, and the net polarization is only about 1%. The observed polarization is 3%, and even without dilution the model produces insufficient polarization. This is a serious consideration, since we do expect that there will be other components to the continuum and line radiation. There might be attenuated and reddened light seen directly from the BLR and the central continuum source; C99 estimate that for 3C 445 the central source is seen through about 2 magnitudes of extinction.

We conclude that the equatorial scattering model in Figure 2 can explain some of the features seen in Type 1 AGN polarization data. Discrepancies remain but these may be resolved in the future by exploring the parameter space of radial and circular motions of the emitters and scatterers.

References

- Cohen, M.H., Ogle, P.M., Tran, H.D., Goodrich, R.W. & Miller, J.S. 1999, *ApJ*, 118, 1963 (C99)
- Goodrich, R.W. & Miller, J.S. 1994, *ApJ*, 434, 82
- Martel, A.R. 1996, Thesis, University of California, Santa Cruz (M96)
- Martel, A.R. 1998, *ApJ*, 508, 657
- Ogle, P.M. 1998, Thesis, California Institute of Technology
- Ogle, P.M., Cohen, M.H., Miller, J.S., Tran, H.D., Goodrich, R.W. & Martel, A.R. 1999, *ApJS*, 125, 1
- Ulvestad, J.S., Wrobel, J.M. & Carilli, C.L. 1999, *ApJ*, 516, 127